PERFORMANCE MEASUREMENTS IN A TRANSIENT TURBINE TEST FACILITY- PRELIMINARY INSTRUMENTATION DEVELOPMENT

N R Atkins, R J Miller, R W Ainsworth Dept. of Engineering Science University of Oxford

ABSTRACT

This paper describes some of the preliminary work that has been carried out in preparation for aerodynamic performance or efficiency measurements in the Oxford Rotor Facility (ORF) (Ainsworth (1988)). The current working section features a 62% scale, 1½ stage, high-pressure shroudless transonic turbine. The turbine is driven by an isentropic light piston tunnel (ILPT). The facility operates in a transient manner with a quasi-steady state run time of approximately 100ms. Engine representative specific speed, pressure ratio, gas-to-wall temperature ratio, Mach and Reynolds numbers are all simulated. This paper outlines solutions to the unique technological issues presented by performance testing in a transient facility.

The three main challenges discussed are the measurement of shaft power, mass-flow rate, and total inlet enthalpy.

INTRODUCTION

This work is part of an on-going program into the development of new instrumentation techniques for use in transient facilities. High bandwidth pressure, entropy and heat transfer instrumentation techniques have been developed in the ORF over the past decade (Ainsworth (1994), Payne (1999), and Thorpe (2000)). Supplemented by the use of unsteady CFD codes, these techniques have enabled the detailed study of the complex phenomena that influence the performance of the turbine. The development of efficiency testing in the ORF will provide a link between the wealth of data on the structure of the loss mechanisms and flow phenomena, and their actual quantitative effect on the overall performance of the turbine stage.

Transient or short duration testing has many advantages over testing in traditional steady flow rigs. The primary aim of this work is to achieve levels of accuracy comparable with steady flow test rigs. Uncertainties in the region of 0.2% to 0.5% are commonly reported. The feasibility of transient performance testing at the MIT Blowdown facility was investigated by Guenette (1989), who concluded that '*turbine aerodynamic performance can be measured in short duration facilities at least as well as conventional rigs'*. Halderman et al (1991) concluded that transient testing could achieve a relative accuracy of ±0.25%. Temperature instrumentation developments have been described by Cattafesta (1988), and more recently by Paniagua (2002). Results of full experimental testing at the MIT Blowdown facility have recently been published by Keogh (2000 and 2002).

The engine representative gas-to-wall temperature ratio of transient test facilities enables the study of heat transfer. Performance testing in transient facilities will allow for the first time the simultaneous study of the performance penalties/gains associated with geometry changes motivated by heat transfer considerations. This type of testing is not possible in traditional adiabatic steady flow rigs.

Whatever the method, the measurement of aerodynamic performance or efficiency requires the measurement of the mass flow rate through the rig, the actual power absorbed by the turbine, and a measurement of the ideal work that could have been liberated for the given operating point, together with an accurate account of the parasitic losses. Preliminary work towards all three will be presented here.

NOMENCLATURE

A_{cal}	Effective area
c_p	Specific heat
c_{ax}	Axial chord
DAQ	Data aquisition
$\dot{H}$	Total enthalpy
J	Polar moment of inertia
p	Static pressure
$\dot{m}$	Mass flow
N	Speed
P	Total pressure
Pr	Pressure ratio
R	Specific gas constant
T	Temperature, Torque
V	Volume
$\dot{W}$	Power
γ	Specific heat ratio
η	Efficiency
ω	Rotational speed

SUBSCRIPTS

0	Total value
1	HP NGV inlet
2	HP NGV exit/HP rotor inlet
3	HP Rotor exit/IP vane inlet
4	IP vane outlet
$\bar{}$	Mass weighted value
tube	Measurement take inside the piston tube
s	Static value
is	Equivalent isentropic, adiabatic value
actual	Measured value

THE OXFORD ROTOR FACILITY (ORF)

Efficiency measurement in the ORF has some unique features. The turbine is un-braked, sweeping through a range of specific speed during the run. The other non-dimensional parameters are kept approximately constant, so testing will yield a curve of efficiency versus specific speed. Considering that the desired resolution of performance between two configurations is of an order of 0.25%, the operation of the ORF rotor provides an elegant solution to the problem of resolving the subtle variations found between the operating points of different configurations (Schobeiri (2000))[1].

When measuring the isentropic, adiabatic efficiency of a stage in a transient manner, heat transfer from the working fluid to the working section must be accounted for (Denton (1993)). The control of heat transfer to areas such as the over-tip casing, and the blade tips themselves is the subject of current research (Shin 2002). In the cold flow of the ORF the total magnitude of this heat flow is estimated to be in the region of 20kW, approximately 1% of the total power liberated from the working fluid. Considering the target resolution of the performance measurement, an error of just ±10% in the prediction of the heat transfer loses would compromise the overall measurement accuracy. The ORF has 135 thin film heat transfer gauges in the areas of interest, as well as a large data set of blade surface measurements. This instrumentation is key to the accurate resolution of aerodynamic performance changes. Traditional steady state rigs do not have the capability to measure heat transfer in the way.

Facility Operation

The next section outlines the pertinent features of the operation of the facility. Prior to a test run the working section and dump tank (figure 1), are evacuated to a pressure of 35 mbar. The piston tube is pressurised to 3.03 bar, and the turbine disc is spun up to 7150rpm using an air motor. To run the tunnel, the 157 bar reservoir gas is used to compress and raise the temperature of the working section gas[2] in front of the piston. At the required pressure the annular gate valve is opened and the gas flows into the working section. The volumetric flow rate out of the driver reservoir is matched to that through the working section, giving a quasi-steady state run time of approximately 100ms. During this time the rotor accelerates by approximately 3000 rpm, passing through its design speed of 8910rpm. A time history of the working section pressure is shown in figure 2. The non-dimensional operating parameters are shown in Table 1.

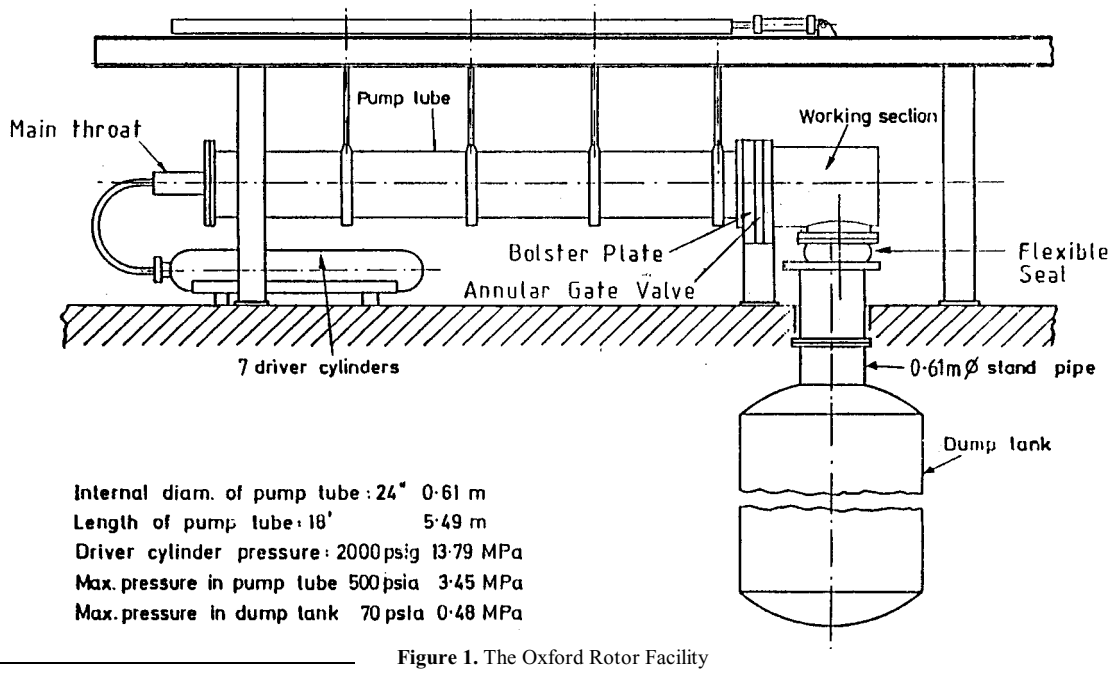

Figure 1. The Oxford Rotor Facility

[1]Facilities that operate with a nominally constant speed such as the MIT Blowdown facility, Epstein (1984), and the Pyestock ILPT, Hilditch (1994), may require more complex testing.

[2] The piston is free, and the compression takes 300ms, hence the process is approximately isentropic.

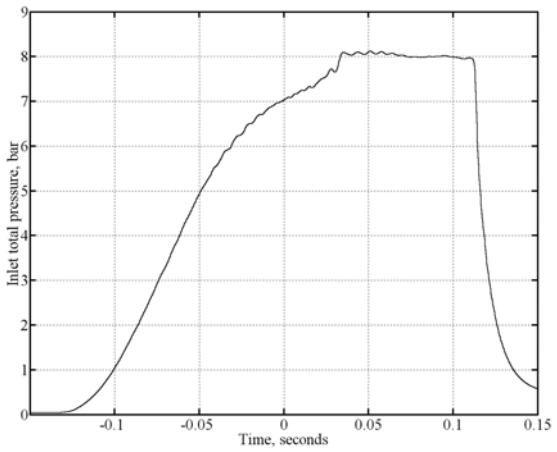

Figure 2. Time history of the stage inlet total pressure

PARAMETER	VALUE
Specific mass flow	7.025×10^{-4} [$kgs^{-1}K^{1/2}$ /bar]
Specific speed	460.5 [$rpm/K^{1/2}$]
Re (based on NGV C_{ax})	2.7×10^{6}
NGV exit mid height Mach No.	0.903
Upstream total temperature	374.4 [K]
Upstream total pressure	8.04 [bar]
Pr (P_{01}/P_{03})	2.75

Table 1. Operating point values

The next section will outline how the actual power absorbed by the turbine will be measured during a test run.

ACTUAL POWER MEASUREMENT

The power absorbed by the turbine at a particular point during the run is given by the following expression:

$$\dot{W}_{actual} = J\left(\frac{d\omega}{dt}\right)\omega + T_{drag}\omega$$

The inertial term has a magnitude of approximately 2.5MW, and the second term represents parasitic drag, including both friction in the bearings, and the aerodynamic drag (or windage) on the rotor disc. Measurement of the parasitic drag forces was made by Sheard (1989) during commissioning of the facility. They have a magnitude of approximately 15 kW, ~0.5% of the inertial power. Error in their measurement (discussed later) represents a bias error, and measurement to an accuracy of a few percent will mean that their effect on the overall accuracy is negligible. The rotational moment of inertia of the complete rotating assembly, *J*, was also measured at 1.633kgm^2 using an accurate tri-filar suspension method. Thus the prime concern is the measurement of the speed and acceleration of the turbine disc. Of the various methods available an optical encoder disc was chosen, being a proven technology in the harsh environment found within the working section.

The three main considerations for the design of the encoder system were accuracy, frequency response, and immunity to noise. The velocity is a direct measurement, but the acceleration is derived by differentiation. The differentiation requires the removal of noise from the velocity signal leading to a direct trade off between absolute accuracy and frequency response. The design philosophy of the system was thus to provide a signal that requires as little smoothing in time as possible for a given bandwidth.

Subtle variations in the operating point are primarily driven by the inlet total conditions. The principal components are ±0.5% at 30Hz due to the finite mass of the piston, and ±0.2% at 150Hz due to the reflected pressure wave that travels through the working section. Although the large inertia of the rotating assembly will act as a low pass filter to these inputs, a target bandwidth of 1kHz was chosen to match the maximum meaningful bandwidth of the rest of the inlet instrumentation (artificially limiting the bandwidth of an individual parameter will lead to spurious phase errors). A typical time history of the speed of the rotor is shown in figure 4.

The encoder disc itself features two concentric discs, one with 600 lines and one with 660 lines mounted directly onto the clamp ring of the turbine disc. The discs were produced using CAD and printed by WTBI Ltd. onto transparent film using a high-resolution laser technique. Iterations were made to account for the thickness of the ink to ensure that the mark space ratio of the encoder strips was as close to 50:50 as possible, in order to avoid problems with the signal processing. A section of the mounted encoder disc is shown below in figure 3.

Figure 3. The encoder disc

The printed film disc was fixed to a rigid base, centred optically on a precision digital read-out lathe and cut into rings. A mandrel was then used to mount the discs concentric to the clamp ring. Considering that the discs are exposed to both high centripetal accelerations and an oil mist from the bearings, the rings are bonded in place using 3M VHB pressure sensitive adhesive, a method that has been proven reliable in this environment.

Encoder design and prototype signal conditioning

Velocity errors due to the relative movement of the disc and pickup[3] are minimised by using two pick up systems 180° apart, and mounting the encoder at the maximum feasible diameter of 0.404m.

For a given level of noise, the faster the rise time of an encoder pulse, the smaller the uncertainty in the position of the edge. To achieve the fastest possible rise times the encoder lines are read using a focused laser spot and a high-speed photodiode. The signal from the photodiode is a square wave with a maximum frequency of about 100kHz. To give accurate edge detection, a very low capacitance photodiode is coupled to a wideband transimpedance amplifier, giving an approximate system bandwidth of 6 MHz. The bandwidth has been achieved by careful design using a Burr Brown OPA655 op-amp and surface mount technology components. The output from the amplifiers is sampled using an Agilent 54625A digital oscilloscope at 20MHz. The sample rate is the maximum available, and provides roughly 10 times over-sampling on the 4th harmonic at 1.1MHz. Data is stored in the on-board memory and then downloaded via a GPIB link to the DAQ computer once the test run is finished. Extremely short rise times in the region of 700ns (approximately 14 samples) have been measured. It is believed that this is limited by the convolution of the spot with the edge of the encoder lines. The bandwidth of the system gives the potential to precisely characterise the encoder disc in order to remove the once per revolution signature (seen in figure 8) due to any residual warping or eccentricity. This will be explored together with more refined signal processing.

Single line system testing

System testing has been carried out on a prototype single channel of the encoder in order to prove the concept and optimise the design. Basic data reduction technique used for the prototype testing are outlined below. A short time, or swept Fourier technique has been used to process the data. The procedure is carried out using MATLAB and is outlined below:

- The data is windowed using a flat-top Hanning window of length 0.25ms. This window is swept along the signal, in 0.25ms steps giving an effective sample rate of 4kHz. A single portion of the data is shown in Figure 5.
- The fundamental frequency of each portion of data is measured using a Discrete Fast Fourier Transform, resulting in the raw speed trace shown in figure 6. The frequency is effectively averaged over each 0.25ms period.
- The raw speed signal is digitally filtered to remove frequency components at the once per revolution frequencies and above to remove residual noise. It is then differentiated using a fourth order numerical scheme to get the acceleration.
- The acceleration is multiplied by the rotational moment of inertia and the speed to give the measured power (Figure 7).

Processed in the manner described above the speed signal has a bandwidth of about 2kHz. However, filtering to remove the once per revolution signal due to the residual eccentricity of the encoders before differentiation limits the bandwidth to approximately 100Hz. The eccentricity signature can be seen centred at about 140Hz, with harmonics at 280Hz, and 560Hz (figure 8). The twin pickups (as well as characterisation of the disc) will remove the eccentricity component as well as providing four times the amount of data for each point of calculated speed. Based on these results the full four-channel system is expected to achieve at least 600Hz, and is currently in manufacture.

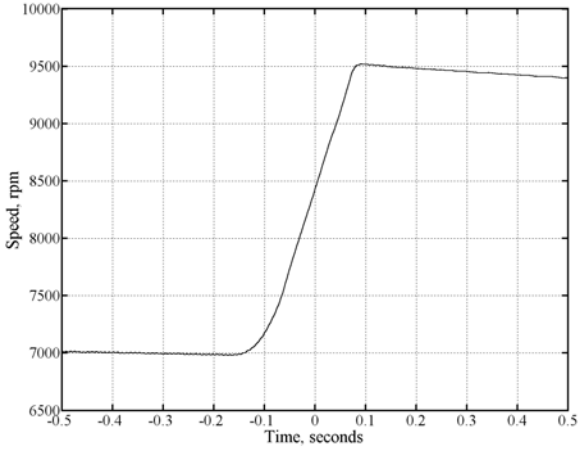

Figure 4. Speed trace of a typical run

[3] Primarily due to eccentricity of the encoders rather than movement of the shaft itself

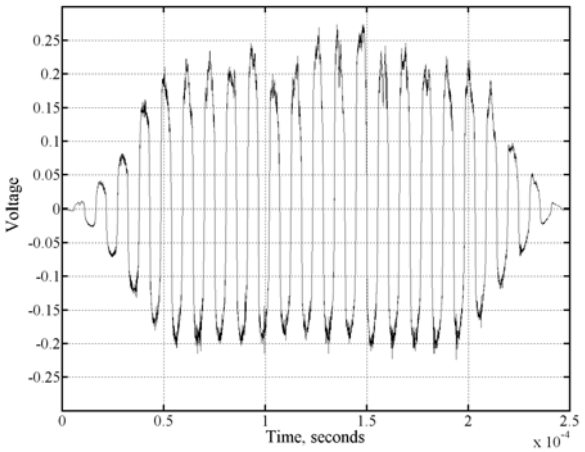

Figure 5. 0.25ms of windowed encoder signal data

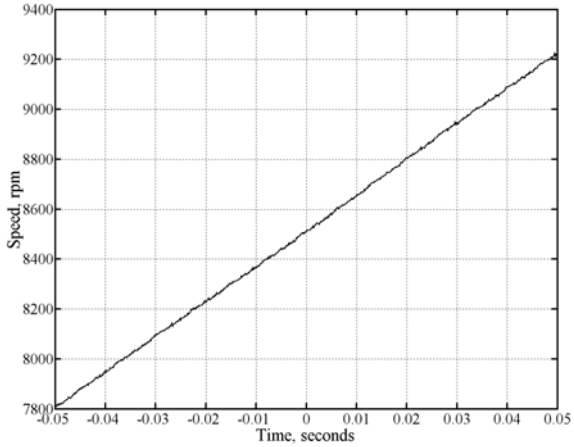

Figure 6. Raw speed data

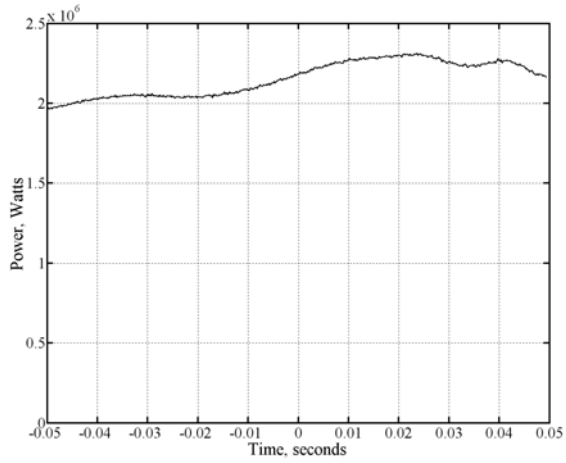

Figure 7. Raw power, derived from filtered velocity data

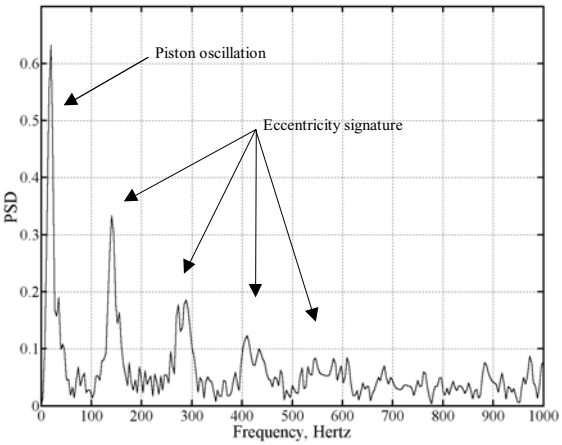

Figure 8. Frequency content of the raw speed signal

Parasitic actual power measurements

The combined bearing drag and rotor disc windage was measured at 15kW during commissioning of the facility (Sheard, (1989)). This represents about 1% of the total power output from the turbine. Further pressure instrumentation has been installed in the bearing cavity and the combined drag torque will be measured using a series of spin down tests. The rotor is allowed to freewheel to rest under a range of pressures; it is braked only by the drag torque which is measured from the deceleration. The range of pressures allows a correlation between the pressure in the cavity and the drag force to be made.

The next section describes the measurement of the ideal power.

IDEAL POWER MEASUREMENT

The ideal power is measured by considering what the total enthalpy drop across the stage would have been if the expansion were isentropic.

$$\dot{W}_{ideal} = \dot{H}_{01} - \dot{H}_{04}$$

Thus:

$$\dot{W}_{ideal} = \dot{m} C_p \overline{T}_{01} \left\{ 1 - \overline{P}_r^{\frac{?-1}{?}} \right\}$$

The measurements $\overline{T}_{01}$ and $\overline{P}_{01}$ represent mass weighted values, the calculation of which will be discussed later. The method of mass flow rate measurement is outlined below.

Mass Flow rate

Subtle variations in the inlet pressure mean that the mass flow rate through the working section is not constant. Thus the measurement plane is situated as close as possible to the rotor to minimise phase errors between the mass-flow rate and the rest of the instrumentation. The technique exploits the venturi between the widest part of the

inlet annulus and the throat plane of the HP NGV's (figure 9). The instrumentation has been calibrated using a blowdown technique. In comparison to other facilities of this type it should be noted that this method is possible in the ORF due to the lack of inlet boundary layer bleeds, and the fact the HP NGV's are very nearly choked. Preliminary testing was carried out with the existing instrumentation in order to check the validity of the method before a full facility strip was under taken. The results are presented here together with the design of the final instrumentation.

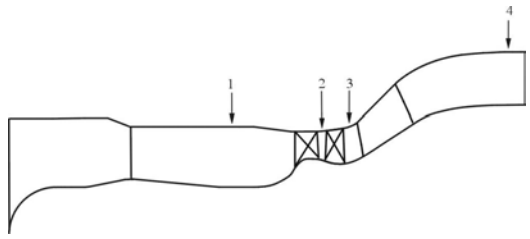

Figure 9. Annulus profile of the ORF

Preliminary testing

The working section instrumentation yields a measurement of the mass flux through the measurement plane; the blowdown calibration technique is used to measure its effective area.

Blowdown calibration

The effective area calibration is made by passing a known mass flow-rate through the measurement plane. This is achieved by removing the piston from the piston tube and using it as a blowdown tank.

The piston tube is pressurised to 9 bar and the gas is allowed to drain through the working section. The mass flow out of the tube is calculated from the ideal gas law by considering a control volume consisting of the piston tube and the inlet annulus up to the measurement plane.

$$\dot{m}_{actual} = \frac{V_{tube}}{R}\frac{d}{dt}\left(\frac{p_{tube}}{T_{tube}}\right)$$

The mass flow rate through the measurement plane is calculated from the following expression:

$$\dot{m} = A_{cal}\, p \left\{ \frac{1}{\overline{T}_s}\left[\left(\frac{\overline{P}_0}{p} \right)^{\frac{\gamma-1}{\gamma}} - 1 \right] \right\}^{\frac{1}{2}}\Bigg|_{plane}$$

By considering continuity through the measurement plane, the effective area A_{cal} is given by:

$$A_{cal} = \frac{\frac{V_{tube}}{R}\frac{d}{dt}\left(\frac{p_{tube}}{T_{tube}}\right)}{p\left\{ \frac{1}{\overline{T}}\left[\left(\frac{\overline{P}_0}{p} \right)^{\frac{\gamma-1}{\gamma}} - 1 \right] \right\}^{\frac{1}{2}}\Bigg|_{plane}}$$

The effective area, A_{cal}, is a function of both the Re and Mach numbers, so the calibration is made when the Mach and Re numbers of the measurement plane are matched in a non-dimensional sense to the run condition. The choice of the final measurement plane is discussed below; being just upstream of the choked HP NGV throat it is insensitive to the flow field of the rotor. The preliminary tests were made with static tappings at the HP NGV exit, and yielded very satisfactory results. The mass-flow rate for a typical run is shown in figure 10. The specific mass flow rate was shown to be repeatable to within ±0.06% across 4 runs (Figure 11). It should be noted that the preliminary measurements were taken with a sixteenth of the final instrumentation. The results have been combined with the results from a detailed pre-test uncertainty analysis in the design of the final instrumentation.

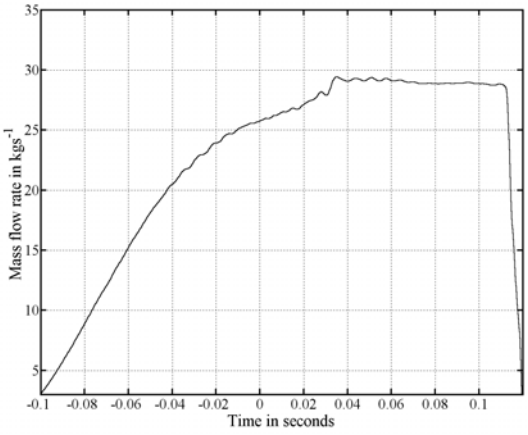

Figure 10. Typical mass flow rate plot

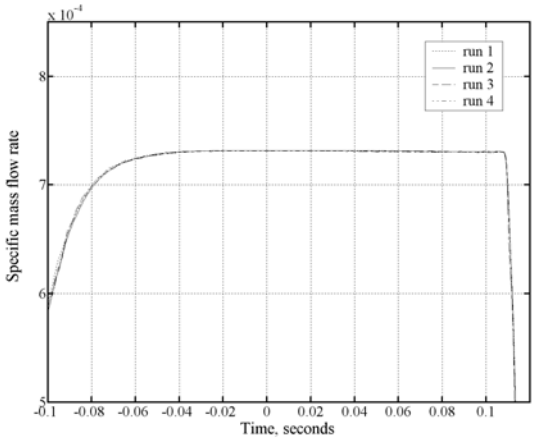

Figure 11. Specific mass flow rate from 4 test runs

Final instrumentation design

The mass flow rate instrumentation must be both de-coupled from changes in the downstream flow field, and as insensitive as possible to measurement error. The results of a detailed uncertainty analysis (see Annex for summary of results) showed that errors in the measurement of pressure would be amplified unless the flow through the measurement plane has a sufficiently high Mach number. Linear cascade data (figure 12a) from a profile based on a mid height section of the current HP NGVs (Nicholson (1985)) shows that the static pressure of positions forward of 90% axial chord on the PS and 30% axial chord on the SS are insensitive to the downstream conditions. They represent the optimum compromise between attenuation of measurement error and downstream insensitivity. The positions were verified with both an UNSTREST CFD solution and data from Mach number profile testing in the current facility Sheard (1989).

Four HP NGV's have been instrumented with an aerodynamic leading edge total pressure taping, and static pressure tappings both PS and SS (figure 12b). The static tappings are situated at 90% and 30% axial chord, both at mid height. The pressure tappings are supplemented with four rakes of four thermocouples distributed around the annulus.

The design of the combined pressure and temperature rakes, their mass weighting and a discussion of the actual transducers and their calibration will be presented in the following sections.

The measurement of mass flow out of the piston tube is achieved using a 4m long rake. It features 6 axially distributed static pressure tappings to check for velocity profiles and 8 thermocouples, 4 of which are distributed radially to check for the presence of a thermal boundary layer. It should be noted that when the flow is at the correct non-dimensional condition (during calibration) the gas in the tube is 10°C below ambient. The thermocouples are aspirated to provide the required time constant.

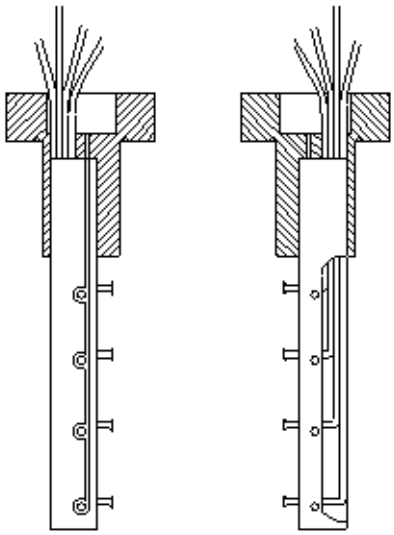

Figure 13. Prototype rakes

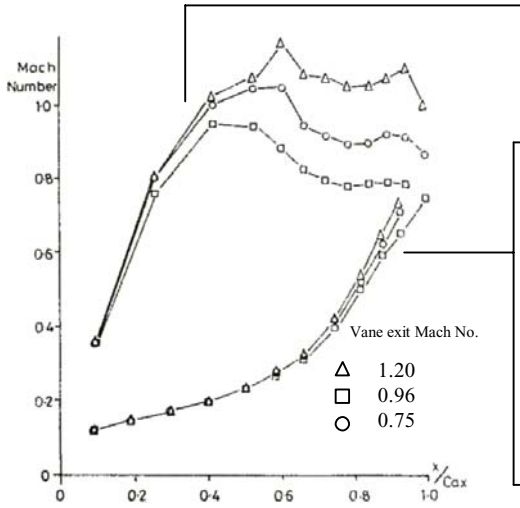

Figure 12a. Vane exit Mach number from Nicholson 2D cascade data

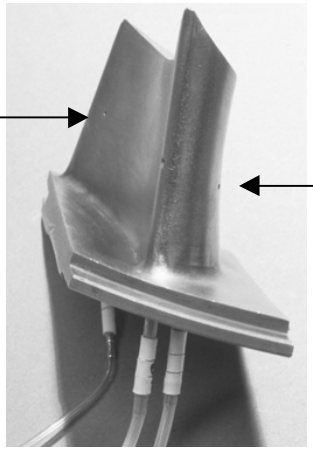

Figure 12b. Instrumented vane

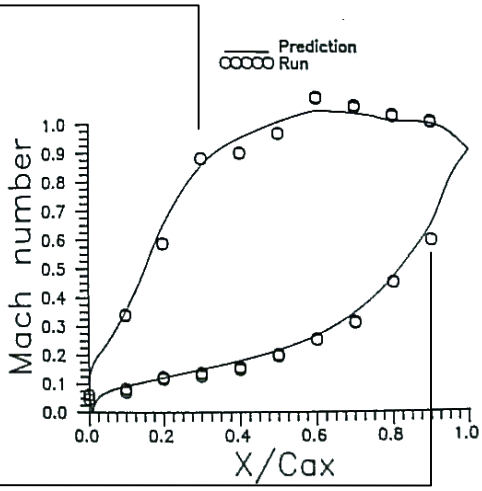

Figure 12c. Sheard 3D data

Aerodynamic Instrumentation

The calculation of ideal power requires the measurement of the inlet total temperature and pressure. As the inlet plane has a profile of mass flux, shown in figure 14, the individual aerodynamic measurements need mass weighting in order to measure the correct total enthalpy flow. The total inlet enthalpy is given by the expression,

$$\dot{H}_{01} = \dot{m} c_p \bar{T}_{01} = \int_{Area} \rho u_{axial} c_p T_{01} dA$$

The mass weighted temperature is defined by the following expression.

$$\bar{T}_{01} = \frac{1}{\dot{m}} \sum_{n=1}^{n=16} (\rho_n u_{axial\,n} A_n) T_{01n}$$

The 16 temperature measurements T_{01n} are positioned radially at the centres of sections of equal annulus area. The 16 weighting terms, $\rho_n u_{axial\,n} A_n$ are calculated from the results of a mass flux survey over the measurement plane shown in figure 14 using the following formula.

$$\rho_n u_{axial\,n} A_n = \frac{1}{T_{01n}} \int_{Area\,n} \rho u_{axial} T_{01} dA_n$$

The ideal total outlet enthalpy is calculated by considering an isentropic expansion across the operating pressure ratio of the stage, thus:

$$\dot{H}_{04} = \dot{m} c_p \bar{T}_{04s} = \dot{m} C_p \bar{T}_{01} \left(\frac{\bar{P}_{01}}{\bar{P}_{04}} \right)^{\frac{\gamma-1}{\gamma}}$$

The pressure measurements are mass weighted in the same way as the temperatures.

The Mach number on this inlet plane is approximately 0.1, so the inlet profile survey is performed using a small pitot-static tube of a standard design, with a 12.7μm thermocouple

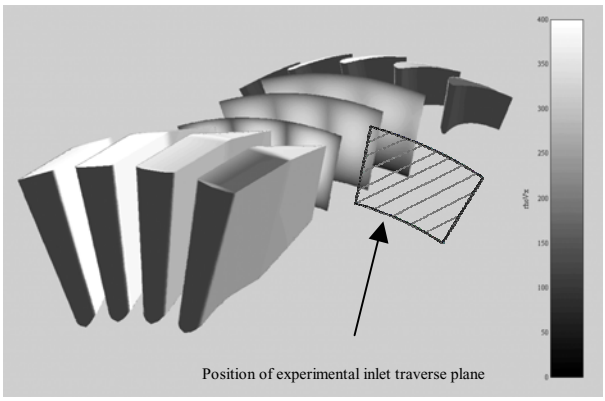

Figure 14. Inlet mass flux profile

mounted on the nose. A detailed hot wire boundary layer survey is also planned.

Total Temperature Rakes

The nature of transient turbine test facilities allows modelling of the correct gas-to-wall temperature ratio, which enables heat transfer studies and the correct modelling of secondary flows. This can lead to unsteady conduction errors in the measurement of temperature. Other considerations for temperature measurement include radiation error, recovery errors, and calibration errors.

Various temperature measurement techniques have been explored in transient test facilities including thin films, optical methods, cold wires and thermocouples, which have been chosen for this work. Although they have a lower frequency response than the other methods, a distinct advantage of thermocouples is the direct nature of their measurement; very low uncertainty levels are possible through simple static calibrations. K type wires have been chosen because of their proven reliability, E type wires are currently being tested, motivated by their higher output and lower overall conductivity. The final instrumentation will use four rakes, with four thermocouples on each. Prototype rakes have been manufactured, and preliminary testing has been carried out. The design methodology is set out below.

Radiation

As radiation errors are in the region of 0.03%, and roughly constant, the added complexity of radiation shields has been avoided. Once compensated for, the radiation error in the actual temperature measurement will be negligible.

Recovery error

The issue of recovery error has been addressed by measuring the temperatures at a plane where the Mach number of the flow is less than 0.1, it is suggested by Stanworth (1962) that a plane thermocouple bead has a recovery factor of about 0.75, corresponding to an error of only 0.03%. Traditional Kiel hoods are thus not required, and their associated drop in frequency response is avoided. Again once compensated for, the recovery error will have a negligible impact on the uncertainty of the temperature measurement.

Unsteady conduction/Frequency response

The issues of unsteady conduction and frequency response have been addressed by the use very thin 12.7μm (0.0005") wires. The L/D ratio of the exposed wires is key to minimising the unsteady conduction (Paniagua (2002)).

The thermocouple junction, wire and ceramic supports have been modelled as a series of linked first order 1-D systems using a Crank–Nicholson finite volume scheme. Initial results suggest that

ceramic supports of 6mm, with 0.5mm of thermocouple wire exposed perpendicular to the flow would be sufficient to give accurate results. This gives the prototype rakes a L/D ratio of approximately 40. The wires are structurally reinforced with a tiny meniscus of cyanoacrylate adhesive as suggested by Lawton (1996). Bench testing was performed with a free jet to check that the fine wires did not deflect excessively under representative aerodynamic loading.

Many heat transfer coefficient correlations exist for thermocouple beads, however due to the difficultly in measuring the bead diameter of a 12.7μm wire thermocouple, it was decided that the modelling should be used as a guide only.

Testing of the prototype rakes (figure 13) has yielded a satisfactory frequency response of about 400 Hz, but the overall level is influenced by conduction errors. It is believed that this is a result of the crude assumptions used to model the flow around the ceramic supports in the 1-D model. This conduction error is currently being addressed by trace heating of the probe supports with Kapton heaters (Guenette (1989)). The rakes have proven themselves to be rugged with no wire breakages to date.

Measurement error

The results of the uncertainty analysis suggest that the temperature measurements need to have a precision error in the region of ±0.1% or ±0.3 K. This has been achieved by careful system calibration. The thermocouples are referenced using an Omega ice-point cell with stability of ±0.04 K and amplified using a National Instruments SCXI 1102C 32-channel thermocouple amplifier. The amplified signals are multiplexed onto a National Instruments PXI 6070E 12bit DAQ card. The amplifiers were chosen for their high temperature stability, important for system calibration. All the wires have been carefully screened, as even low levels of pickup become a problem at this level of accuracy. The amplifiers have built in 10 kHz anti-alias filters, the DAQ card allows a sample rate of 20kHz, giving a satisfactory 10 times over-sampling on the 1 kHz maximum likely bandwidth of the temperature signals. This both improves resolution and reduces the problem of channel skew associated with the multiplexed DAQ. The calibration of the thermocouples to the required accuracy is discussed below.

Calibration

Each rake will be calibrated in an Isotech Venus stirred liquid bath by comparison against a UKAS calibrated semi-standard platinum resistance thermometer. The resistance of the reference thermometer is measured by a 4-wire method on an Agilent 34970A DVM. Both the bath and the DVM are controlled by LabVIEW software across a GPIB link, giving a fully automated calibration system. To achieve the required levels of uncertainty the entire signal chain of each channel is calibrated as a unique system. This includes the actual measurement junction, extension wires, plugs, reference junctions and the amplifier/DAQ channel. The error budget for the calibration system is shown in the table 2 below:

ERROR	VALUE
Worst case non-uniformity in calibration volume	± 0.03K
Thermometer accuracy	± 0.01K
Meter accuracy	± 0.015%
CJ stability (N.B abs level measured with PRT)	± 0.04K
Total calibration uncertainty	**± 0.02%**

Table 2. Temperature calibration error budget

During testing, additional errors are introduced by the temperature coefficient of the amplifier/DAQ channel, and drift of the junctions themselves. Thermocouple drift includes the effects of work hardening, ageing, and inhomogeneity (Kinzie (1973)**)**. These effects are comparatively small, but should not be ignored. The automated calibration system enables frequent re-calibration, and a suitable re-calibration interval (expected to be of the order of a few months) will be found over time. It is expected that the calibration uncertainty of ±0.02% will be more than sufficient to achieve the target temperature measurement uncertainty of ±0.1%.

Pressure rakes

Four bell-mouth pitot tubes are mounted on each inlet rake (figure 13). The length of tubing to the transducers has been kept below 15cm to maintain the desired frequency response**.** The pressure transducers are calibrated using a Druck DPI515 pressure controller. The process is controlled by NI LabVIEW software over a GPIB link. The transducers themselves are plumbed with quick-disconnects such that a full calibration can be performed in approximately 5 minutes. This means that the calibration can be performed both before and after each test run, removing the need for complex environmental stabilisation of the sensors. Thorough testing has been performed on a batch of Sensortechnics PXM series transducers. Again, each signal chain is calibrated as a unique system. Many calibration cycles have been carried out, and worst-case repeatabilities of about ±0.01% have been achieved across six calibration cycles. This is approximately equal to the measurement accuracy of the calibrator and an order of magnitude down on the target precision uncertainty of ±0.2%. The repeatability of a single set point is shown for four successive calibrations in figure 15 below. The

lines represent a second order fit to the 46 calibration points, and the crosses are the actual measured voltages. The error bar is set at the target precision uncertainty of ±0.1% for the purpose of illustration. The pressure transducer output signals are filtered using MAXIM MAX281 zero dc error 5th order anti-alias Bessel filters at 2.5kHz. The signals are then sampled directly at 18 kHz, using a differential input, on NI PXI 6071E DAQ cards. Additional signal conditioning is not required as the DAQ cards feature high-specification programmable gain instrumentation amplifiers, which map the 100mV transducer outputs onto the full scale of the analog to digital converters.

DAQ

Both the DAQ and the GPIB communications are performed by a 150-channel National Instruments PXI system. The system does not feature true simultaneous sampling, but the DAQ cards are fast enough to allow approximately ten times over sampling on all channels, which reduces the problem of channel skew. The system is controlled by a standard PC (running LabVIEW software) via a 100MB/s fiber-optic link. This allows the DAQ cards to be situated in very close proximity to the transducers; preliminary testing has shown very low levels of noise.

CONCLUSIONS

This paper has presented some of the preliminary instrumentation developments towards aerodynamic performance measurement in the Oxford Rotor Facility. Prototype systems to measure the rotor speed, acceleration, mass flow rate, and inlet conditions have been designed and thoroughly tested. The results indicate that performance testing with a relative resolution in the region of ±0.25% will be possible in the Oxford Rotor Facility.

ACKNOWLEDGMENTS

The continued support of Kevin Grindrod, Nigel Brett, Rob Miller and Steve Thorpe is gratefully acknowledged, as well as Rolls Royce PLC for providing the funding for this work.

REFERENCES

Abernethy, R.B., Benedict, R.P, and Dowell, R.B., ASME Measurement Uncertainty, Trans. of the ASME J. of Fluids Engineering Vol. 107 1985

Ainsworth, R. W., Allen, J. L., Batt, J. J. M., The development of tast response aerodynamic probes for flow measurements in turbomachinery, ASME paper 94-GT-23

Ainsworth, R.W., Schultz, D. L., Davies, M. R. D. Forth, C. J. P., Hilditch, M. A., Oldfield, M. L. G., and Sheard, A. G., A transient facility for the stuffy of thermofluid-dynamics under engine representative conditions. ASME paper 88-GT-144

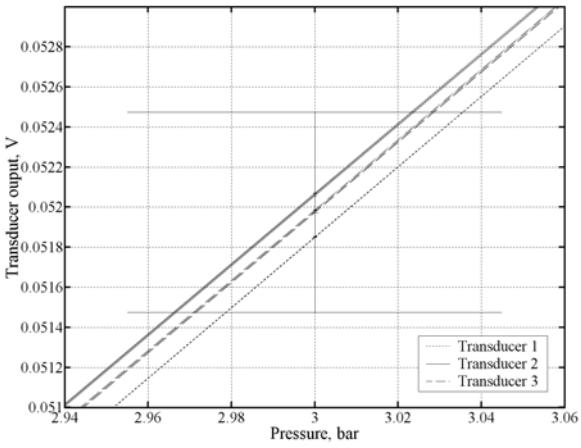

Figure 8. Repeatability of Sensortechnics PXM series sensors

Denton J (1993) "Loss mechanisms in turbomachines" ASME journal of turbomachines vol. 115 pp 621-656

Cattafesta, L. N., Epstein, A. H., "Gas Temperature Measurement in Short Duration Turbomachinery Test Facilities", AIAA-88-3039 1988

Epstein, A.H., Guenette, G.R. and Norton, R.J.G., The MIT Blowdown turbine Facility, ASME Paper 84-GT-116, 1984

Guenette, G.R. Epstein, A.H., Ito, E. Turbine Aerodynamic performance measurements in short duration facilities, AIAA/ASME/SAE/ASEE 25th Joint Prop. Conf. AIAA-89-2690, 1989

Hilditch, M.A., Fowler, A, Jones T.V., Chana, K.S., Oldfield, M.L.G., Ainsworth, R.W., Hogg, S.I., Anderson, S.J. and Smith, G.C. Installation of a Turbine Stage in the Pyestock Isentropic Light Piston Facility. ASME Paper 94-GT-277, 1994

Halderman C. et al "Uncertainty analysis of turbine aerodynamic performance measurements in short duration facilities" AIAA/SAE/ASME/ASEE 27th Joint propulsion conference, 1991

Keogh, R.C., Guenette G.R., Aerodynamic Performance Measurements of a Fully-Scaled Turbine in a Short Duration Facility. Proc. of ASME TURBOEXPO 2000, Munich Germany 2000-GT-486, May 8-11, 2000

Keogh, R.C., Guenette G.R., Aerodynamic Performance Measurements of a Film-Cooled Turbine Stage – Experimental results. Proc. of ASME TURBOEXPO 2002,Amsterdam, The Netherlands GT-2002-30344, June 3-6, 2002

Kinzie, P. A., Thermocouple temperature measurement. John Wiley & Sons, New York, 1973.

Paniagua, G., Dénos, R., Oropesa, M. Thermocouple probes for accurate temperature measurements in short duration facilities. Proc. of ASME TURBOEXPO 2002,Amsterdam, The Netherlands GT-2002-30043, June 3-6, 2002

Payne, S.J. Unsteady Loss in a high pressure turbine stage. D.Phil Thesis Oxford University, 2001

Sieverding, C.H. and Arts, T. The VKI compression tube annular cascade facility. ASME Paper 92-GT-336, 1992

Sheard, A.G., Aerodynamic and Mechanical Performance of a High Pressure Turbine Stage in a Transient Wind Tunnel**.** D.Phil Thesis Oxford University, 1989

Stanworth, C. G., Suction Pyrometers, Proc. of the Symp. on Some developments in techniques for temperature measurement. IMechE London 26th April, 1962

Thorpe, S. J. Yoshino, S., Ainsworth, R.W., "Fabrication and calibration techniques for turbine rotor tip heat transfer gauges." Proceedings of the XVth Symposium on Measuring Techniques for Transonic and Supersonic Flows in Cascades and Turbomachines. Florence, 21-22 September 2000

ANNEX

The precision errors from the detailed pre-test uncertainty analysis are summarized in the tables below. The calculations are based on the method of Abernathy (1985). The precision index given by:

$$\frac{S_{95}}{\sqrt{N}}\%$$

Where N is the number of sensors and S_{95} is 0.2% for pressure measurements and 0.1% for temperature measurements. C is the error coefficient representing the amplification of the error in the relevant data reduction equation.

η	N	$\frac{S_{95}}{\sqrt{N}}$ %	C	P_{95} %
J	n/a	N/a	1	n/a
$\dot{\omega}$	4	0.200	1	0.200
ω	4	0.100	1	0.100
$\dot{m}$, Table B	n/a	0.078	1	0.078
P_r	32	0.018	-1.14	-0.020
T_{01}	16	0.025	1	0.025
$T_{drag}\omega$	n/a	1	0.01	0.010
			TOTAL	**±0.24**

Table A. The efficiency precision error

$\dot{m}$	N	$\frac{S_{95}}{\sqrt{N}}$ %	C	P_{95} %
A_{cal} , Table C	n/a	0.057	1	0.057
p_{plane}	12	0.058	0.25	0.014
P_{plane}	16	0.050	1	0.050
T_{01}	16	0.025	-0.5	-0.013
			TOTAL	**±0.078**

Table B. The mass flow rate precision error

A_{cal}	N	$\frac{S_{95}}{\sqrt{N}}$ %	C	P_{95} %
V	n/a	n/a	1	n/a
R	n/a	n/a	-1	n/a
p_{tube}	6	0.082	0.206	0.017
T_{tube}	8	0.035	1	0.035
p_{plane}	12	0.058	-0.205	-0.012
P_{plane}	16	0.050	0.75	0.038
T_s	16	0.025	-0.5	-0.0125
			TOTAL	**±0.057**

Table C. The effective area calibration precision error